Supporting Information

for *Adv. Funct. Mater.,* DOI: 10.1002/adfm.201706448

Spatially Resolved Electric-Field Manipulation of Magnetism for CoFeB Mesoscopic Discs on Ferroelectrics

*You Ba, Yan Liu, Peisen Li, Liang Wu, John Unguris, Daniel T. Pierce, Danni Yang, Ce Feng, Yike Zhang, Hao Wu, Dalai Li, Yuansi Chang, Jinxing Zhang, Xiufeng Han, Jianwang Cai, Ce-Wen Nan, and Yonggang Zhao**

Supporting Information For:

Spatially-Resolved Electric-Field Manipulation of Magnetism for CoFeB Mesoscopic Discs on Ferroelectrics

*You Ba, Yan Liu, Peisen Li, Liang Wu, John Unguris, Daniel T. Pierce, Danni Yang, Ce Feng, Yike Zhang, Hao Wu, Dalai Li, Yuansi Chang, Jinxing Zhang, Xiufeng Han, Jianwang Cai, Ce-Wen Nan and Yonggang Zhao**

Prof. Y. Zhao, Y. Ba, Dr. Y. Liu, Dr. P. Li, C. Feng, Y. Zhang
Department of Physics and State Key Laboratory of Low-Dimensional Quantum Physics
Tsinghua University
Beijing 100084, China
E-mail: ygzhao@tsinghua.edu.cn

Prof. Y. Zhao, Y. Ba, Dr. Y. Liu, Dr. P. Li, C. Feng, Y. Zhang
Collaborative Innovation Center of Quantum Matter
Beijing 100084, China

L. Wu, Prof. C. Nan
School of Materials Science and Engineering and State Key Lab of New Ceramics and Fine Processing
Tsinghua University
Beijing 100084, China

Dr. John Unguris, Dr. Daniel T. Pierce
Center for Nanoscale Science and Technology
National Institute of Standards and Technology
MD 20899, Gaithersburg

D. Yang, Prof. J. Zhang
Department of Physics
Beijing Normal University
Beijing 100875, China

Dr. H. Wu, Dr. D. Li, Y. Chang, Prof. X. Han, Prof. J. Cai
Beijing National Laboratory for Condensed Matter Physics
Institute of Physics, Chinese Academy of Sciences
Beijing 100190, China

Dr. Y. Liu
Key Laboratory of Space Utilization, Technology and Engineering Center for Space Utilization
Chinese Academy of Sciences
Beijing 100094, China

Dr. P. Li
College of Mechatronics and Automation
National University of Defense Technology
Changsha 410073, China

Keywords: electric-field control of magnetism, multiferroic heterostructure, CoFeB discs, ferroelectric domain switching

S1. Schematic of the sample configuration

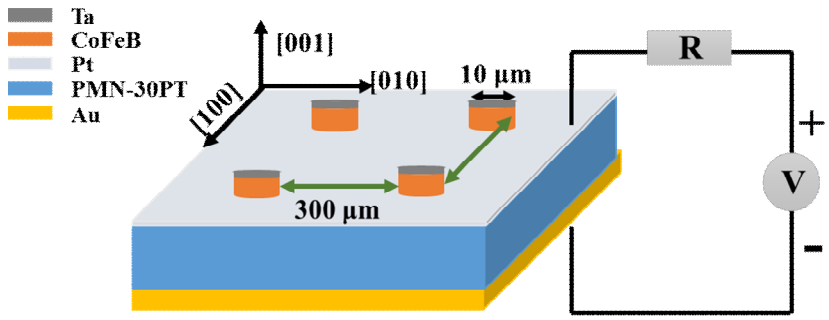

Figure S1. Schematic of the sample configuration.

S2. Three types of FE domain switching in the as-grown PMN-PT

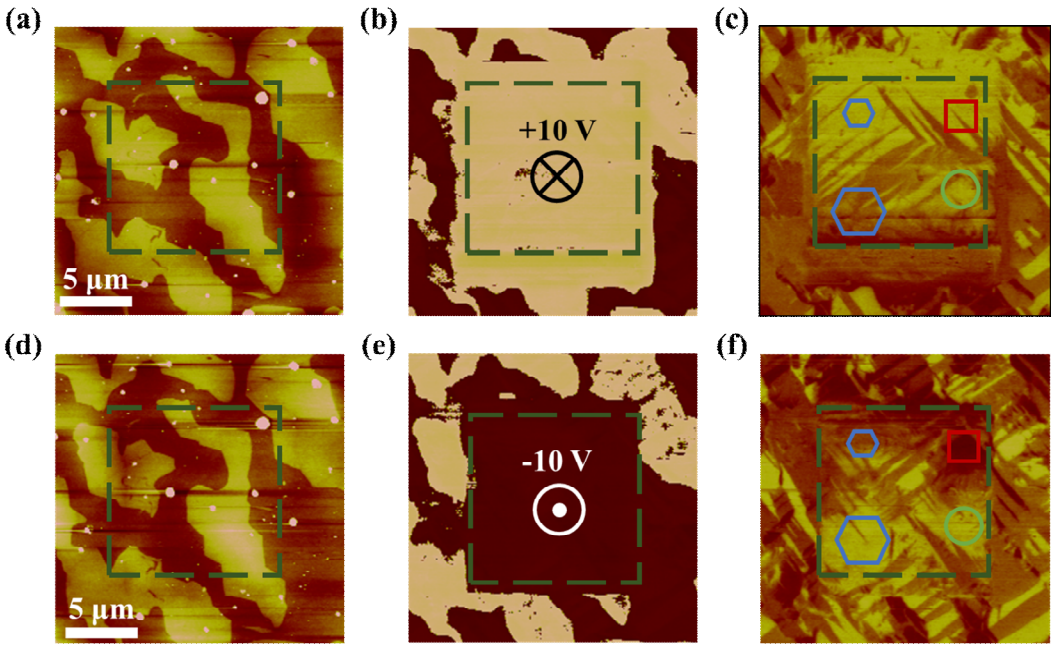

Figure S2. a,d) The topography images, b,e) The out-of-plane phase PFM images, c,f) The in-plane cases after poling with the PFM tip at +10 V and -10 V dc voltage, respectively. Three types of switching can be recognized with the blue hexagon, green circle and red square indicating the 109°, 71° and 180° switching, respectively.

Figure S2 shows the three types of FE domain switching in the as-grown PMN-PT. Every row (from left to right) shows the topography, out-of-plane PFM (OP-PFM) image and in-plane PFM (IP-PFM) image. After poling a 12 μm by 12 μm square in the center area of 20 μm by 20 μm visual field with a +10 V/-10 V dc voltage biased with the tip, the color of the OP-PFM image (Figure S2b

and S2e) changes to white/black indicating the out-of-plane polarization components are switched downward/upward. Combined with the changes of IP-PFM (Figure S2c and S2f), 109°, 71° and 180° switching can be distinguished. The detailed analysis of polarization can be found in our previous work.[1]

S3. P-E loops measured by two methods

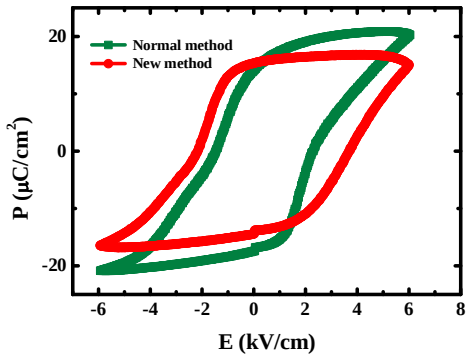

Figure S3. P-E loops measured by the normal method (olive curve) and our new method (red curve), respectively.

To determine the size of the FE domains after applying an electric field, we use a removable conductive membrane as the top electrode to contact closely with PMN-PT without using adhesive, and a Au film sputtered on the bottom of PMN-PT as the bottom-electrode. After polarizing the PMN-PT with electric field of ±6 kV/cm, we removed the top-electrode to get the PFM images for the different remanent polarized states (Figure 1). Before the PFM test, we measured the polarization versus electric field (P-E) hysteresis loop of PMN-PT to check if the top-electrode of flexible conductive membrane is effective to polarize the PMN-PT. The P-E loops measured by two methods are shown in Figure S3. The olive curve was obtained by using the normal method with Au film electrodes sputtered on both sides of the PMN-PT. The red curve was obtained by using the new flexible conductive membrane method. The results indicate that, compared with the normal polarization method with the sputtered Au as the top-electrode, our new method gives a comparable saturation polarization (P_{max}) and the ferroelectric coercive field (E_c), suggesting that the electric field has been effectively applied to the PMN-PT. The slight decrease of P_{max} and increase of E_c

could be attributed to the reduced effective area of the flexible conductive membrane contacting with PMN-PT and the minor gap between them, respectively. Even so, our new polarization method is still useful for determining the size of FE domains.

S4. Data processing of ROT-MOKE

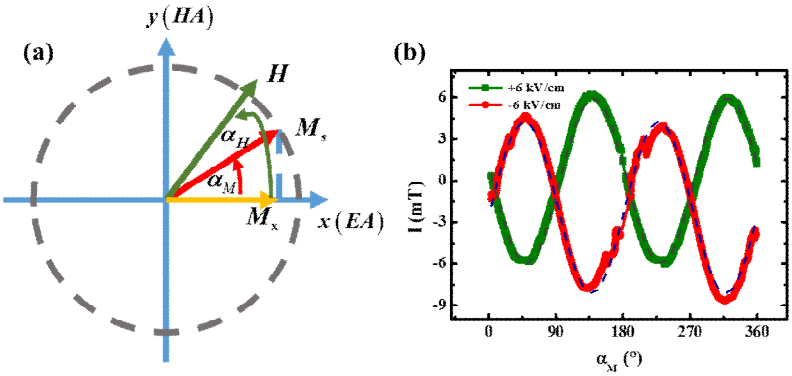

Figure S4. a) The schematic of ROT-MOKE principle. b) Experimental data (solid curves) and fitting curves (dashed curves).

The schematic of ROT-MOKE principle is shown in Figure S4a. During the ROT-MOKE measurement, a rotating field larger than the effective magnetic anisotropy and coercive field is applied to secure a single domain state of the sample for any direction of the in-plane field. Thus, we can assume a Stoner-Wohlfarth like magnetization reversal, in which a simple mathematical description of the magnetization rotation can be used.[2, 3] If there is only a uniform and uniaxial in-plane anisotropy, the energy density e is given by

$$e = \frac{E}{V} = -M_s H \cos(\alpha_H - \alpha_M) + K_U \sin^2 \alpha_M \qquad \text{(S1)}$$

where K_U is the uniaxial anisotropy, M_s the saturation magnetization, V the volume of the magnetic layer, H the applied field strength, α_H the angle between the easy (or hard) axis and the applied field, α_M the angle between the easy (or hard) axis and magnetization. The equilibrium solution for the magnetization can be obtained by differentiating Eq. (S1) resulting in

$$HM_s \sin\left(\alpha_H - \alpha_M\right) = K_U \sin 2\alpha_M \tag{S2}$$

The term

$$L\left(\alpha_H\left(\alpha_M\right)\right) = HVM_s \sin\left(\alpha_H - \alpha_M\right) \tag{S3}$$

is a torque, which is usually determined by torque magnetometry. Here we are able to determine a related value by ROT-MOKE by simultaneous determination of the two angles α_H and α_M, and with the usual definition $H_K = 2K_U / \mu_0 M_s$ (μ_0 is the vacuum permeability), we obtain the following simplified form

$$l\left(\alpha_M\right) = H \sin\left(\alpha_H - \alpha_M\right) = \frac{1}{2} H_K \sin 2\alpha_M \tag{S4}$$

H_K can therefore be deduced from the curve of $l\left(\alpha_M\right)$ versus α_M. Figure S4b shows two typical torque curves of the ROT-MOKE measurement, from which we can obtain the angle of MEA of 96°/3° and the effective magnetic anisotropy field $\mu_0 H_K$ of 12.0 mT/12.4 mT under +6 kV/cm and -6 kV/cm, respectively, by fitting the equation $l\left(\alpha_M\right) = H \sin\left(\alpha_H - \alpha_M\right) = \frac{1}{2} H_K \sin 2\alpha_M$. Obviously, a 90° rotation of the MEA can be deduced from ROT-MOKE.

S5. Angular dependence of coercive field with in situ electric field

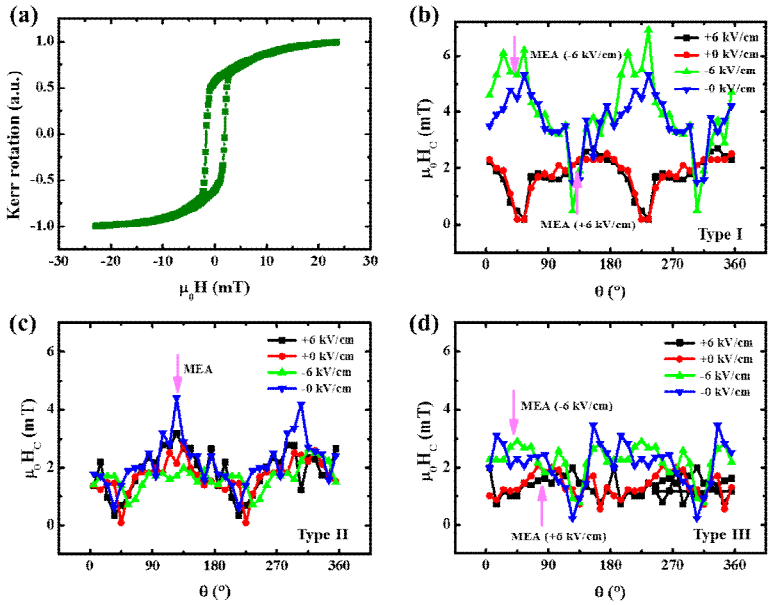

Figure S5. a) A representative Kerr loop. b,c,d) Three different angular dependences of coercive field with in situ electric fields (H_c-θ, θ is the angle between the applied magnetic field and the [100] direction) corresponding to the three types of unique magnetic responses to electric field discussed in the main text. The single standard deviation uncertainty, based on repeated $\mu_0 H_c$ measurements, was less than 0.6 mT. The pink arrows denote the MEA, which is deduced from *Mr/Ms* shown in Figure 2.

S6. SEMPA images of the three types of discs under different electric fields

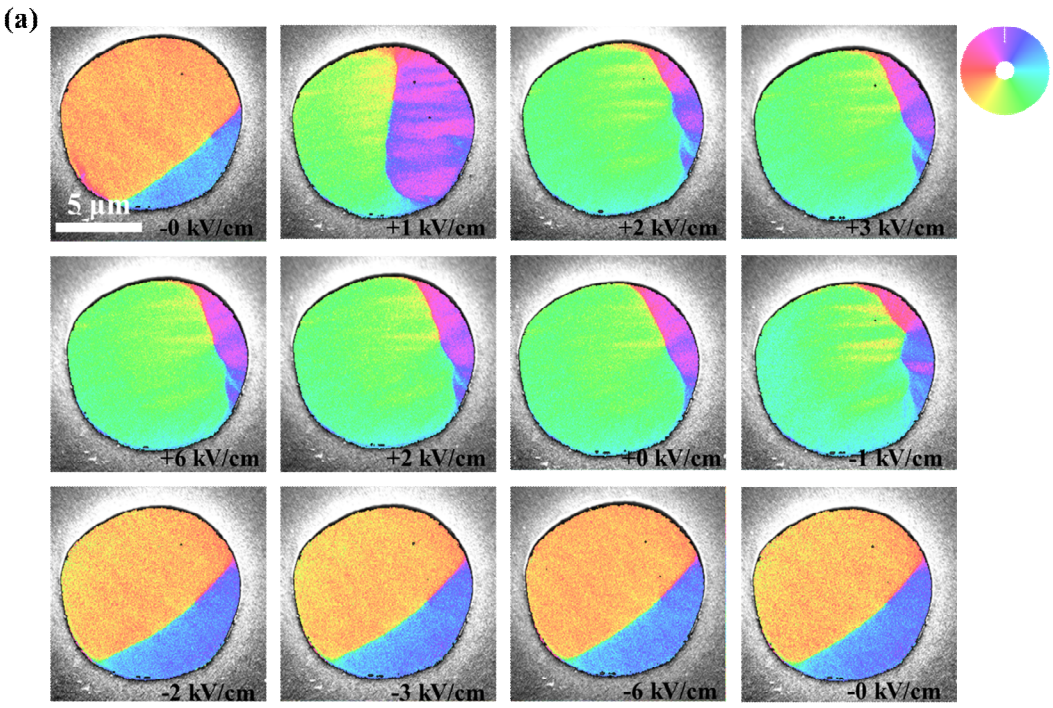
(a)
5 μm
-0 kV/cm
+1 kV/cm
+2 kV/cm
+3 kV/cm
+6 kV/cm
+2 kV/cm
+0 kV/cm
-1 kV/cm
-2 kV/cm
-3 kV/cm
-6 kV/cm
-0 kV/cm

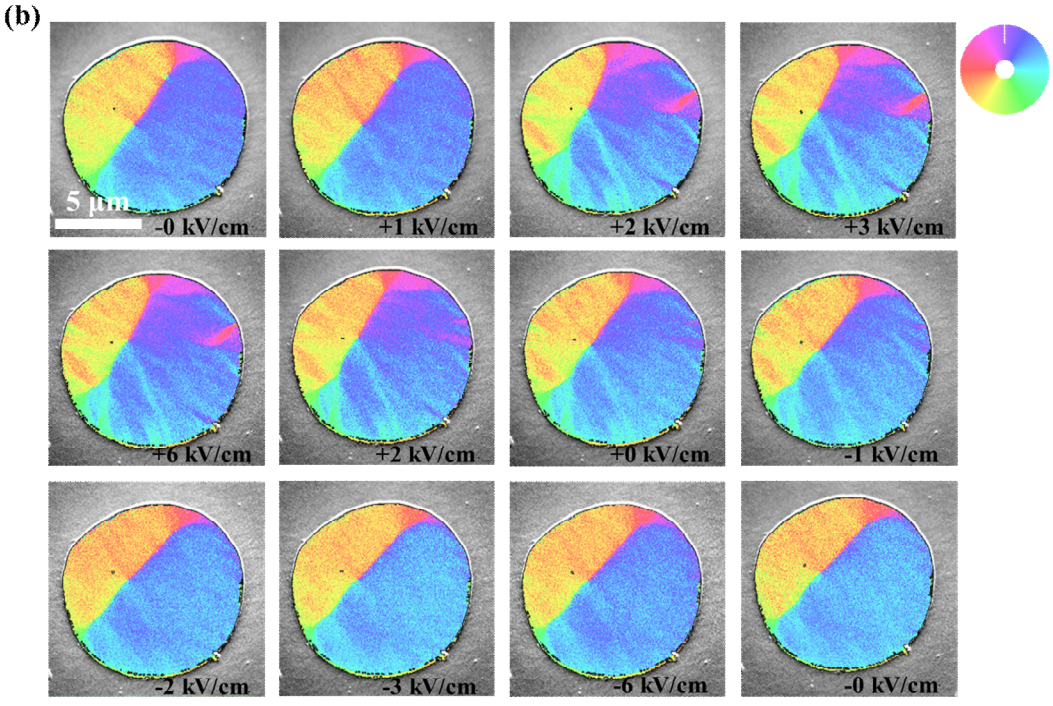
(b)
5 μm
-0 kV/cm
+1 kV/cm
+2 kV/cm
+3 kV/cm
+6 kV/cm
+2 kV/cm
+0 kV/cm
-1 kV/cm
-2 kV/cm
-3 kV/cm
-6 kV/cm
-0 kV/cm

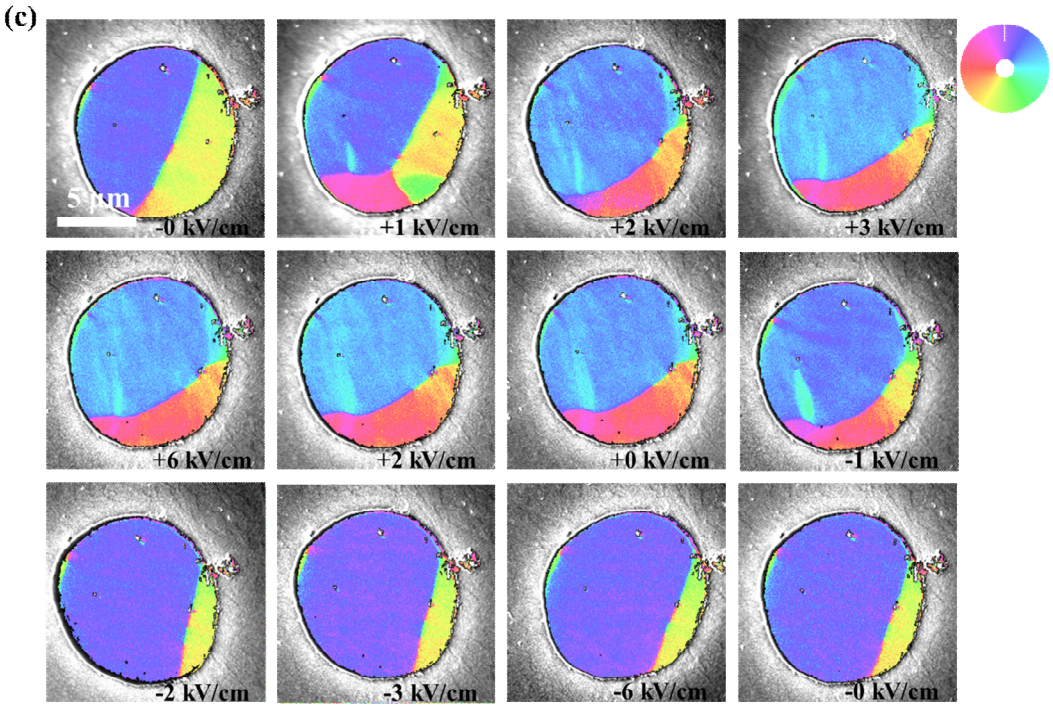

Figure S6. a,b,c) SEMPA images of the three types of discs (type I, type II and type III, respectively) under different electric fields.

S7. Rotation process of magnetic moment vectors

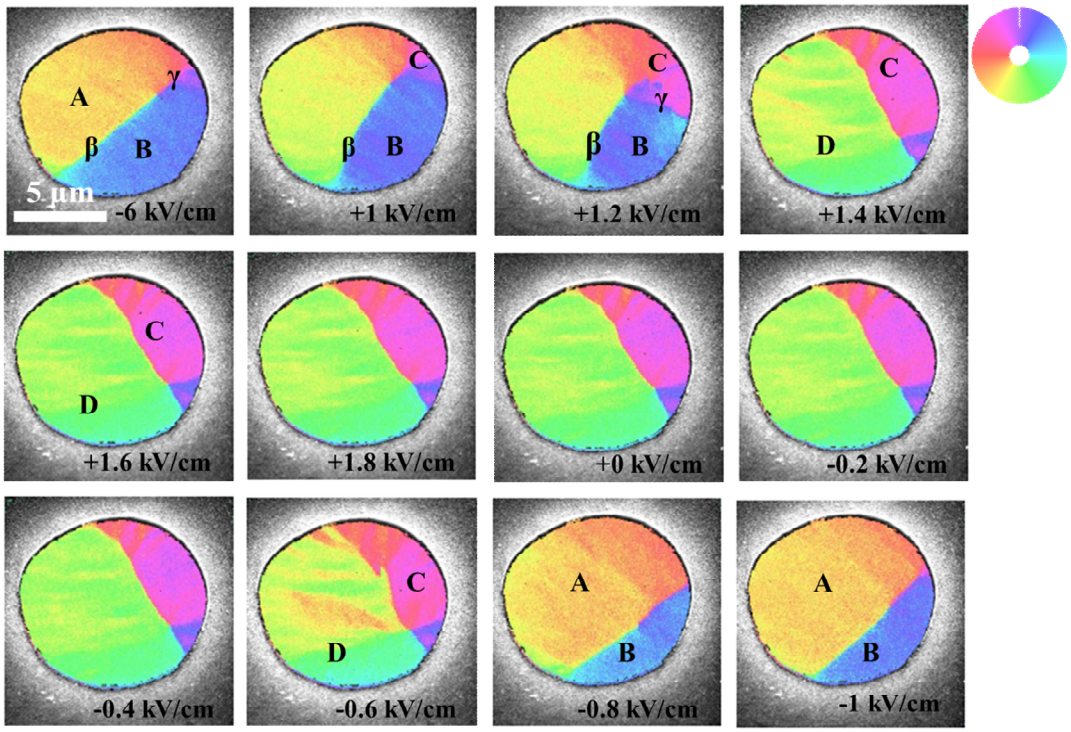

Figure S7. SEMPA images under different electric fields. The magnetization directions in the SEMPA images are given by the color wheel. A, B, C and D indicate different FM domains, and β and γ indicate different FM domain walls.

Figure S7 shows the rotation process of magnetic moment vectors. The magnetic moment rotation is nonvolatile and occurs between +1.2 kV/cm and -0.6 kV/cm. A detailed description is as follows. When E = -6 kV/cm, the disc shows two FM domains (denoted as A-domain and B-domain) with the same MEA, resulting in a 180°-Neel domain wall. The 180°-Neel domain wall is divided into two parts with different chiralities, labeled as the β-domain wall and γ-domain wall. The magnetic moment does not change until the electric field is increased to +1 kV/cm at which point the magnetic moments of A-domain and B-domain begin to rotate and C-domain appears. As the electric field is increased to +1.2 kV/cm, the γ-domain wall moves downward resulting in the expanding of C-domain and the shrinking of B-domain, and in the meanwhile, the direction of A-domain continues to rotate. The magnetic rotation ends up at +1.4 kV/cm with two new domains, C-domain and D-domain. And it changes little with further increase of electric field. From +6 kV/cm to -6 kV/cm, the change happens at -0.6 kV/cm, at which D-domain starts to rotate and B-domain appears due to the magnetic moment rotation and domain wall motion. The original A-domain and B-domain appear and stay stable at -0.8 kV/cm. The rotation process is similar to the former but is more rapid and the critical electric field is also different. The magnetic rotation is mainly driven by the strain-induced magnetostriction effect. The strain curve is usually asymmetric,[4] which may account for the minor difference of the rotation process under the positive and negative electric fields and the different critical electric fields at which magnetic moment rotation starts.

S8. MFM images for E = +0 kV/cm and E = -0 kV/cm

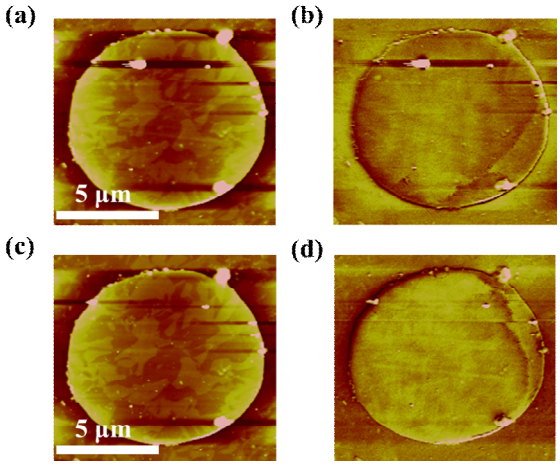

Figure S8. a,c) The topography images. b,d) MFM contrast for the case of E = +0 kV/cm and E = -0 kV/cm, respectively.

The topography images after the sample was polarized by positive and negative electric fields show that the topography of the disc has not been affected by the electric fields. A clear change of magnetic domain wall can be found by comparing Figure S8b with S8d, which reveals the change of magnetism by electric fields on the mesoscale. The detailed information about the rotation of the in-plane magnetic-moment vectors has been presented in the main text and S7 with the SEMPA images.

S9. Separation of the *loop-like* and *butterfly-like* strains

According to our previous report, the asymmetric *butterfly-like* S-E curve is composed of the symmetric *butterfly-like* and antisymmetric *loop-like* curves, and the S-E curve can be divided into two curves based on their different symmetries.[4] To be specific, if we define the S-E curve as functions of $f = S\text{train}(E)$ and $f^* = S\text{train}(-E)$ under the positive and negative electric fields, respectively, then the antisymmetric and the symmetric parts can be obtained as $f_A = \left[S\text{train}(E) - S\text{train}(-E)\right]/2$ and $f_S = \left[S\text{train}(E) + S\text{train}(-E)\right]/2$. The antisymmetric and symmetric S-E curves deduced from Figure 4b are shown in Figure 4c, denoted as "Loop" and "Butterfly", respectively (olive and red curves).

S10. Polarization reversal paths of the previous reports

Some studies claimed that M_A and M_C were found in a (001)-oriented PMN-PT or PZN-PT single crystal near the MPB when poled in the [001] direction, while M_B was mostly found for the (011)-oriented crystals when poled in the [011] direction.[5-7] Bai et al. found the R-M_A-M_C-T polarization rotation path in a (001) PMN-30PT, and no M_B phase.[8] Chien et al. observed M_B phase in a (001) PMN-24PT at high electric fields.[9] Liu et al. recently found a monoclinic polarization rotation of R-M_A-M_B in PMN-32.5PT ceramics at 8 kV/cm.[10] The electric fields in the above studies were unipolar, different from the bipolar-electric-fields in our work. There is only one work concerning the bipolar-electric-field-induced polarization rotation path in a (001) PMN-PT.[11] Fang et al. studied the in-plane cyclic-electric-field-induced polarization rotation and multiphase coexistence for a (001) PMN-32PT and found the R phase turned to the M_C phase after poling, and then systematically studied the M_C phase polarization rotation path under cyclic electric fields.[11] This work is also different from ours, because the electric fields in our work are perpendicular to the surface, instead of in-plane, and the PMN-30PT composition used in our work is different from that of Fang et al.

References

[1] S. Zhang, Y. G. Zhao, P. S. Li, J. J. Yang, S. Rizwan, J. X. Zhang, J. Seidel, T. L. Qu, Y. J. Yang, Z. L. Luo, Q. He, T. Zou, Q. P. Chen, J. W. Wang, L. F. Yang, Y. Sun, Y. Z. Wu, X. Xiao, X. F. Jin, J. Huang, C. Gao, X. F. Han, R. Ramesh, *Phys. Rev. Lett.* **2012**, *108*, 137203.

[2] R. Mattheis, G. Quednau, *J. Magn. Magn. Mater.* **1999**, *205*, 143.

[3] S. Zhang, Y. Zhao, X. Xiao, Y. Wu, S. Rizwan, L. Yang, P. Li, J. Wang, M. Zhu, H. Zhang, X. Jin, X. Han, *Sci. Rep.* **2014**, *4*, 3727.

[4] L. Yang, Y. Zhao, S. Zhang, P. Li, Y. Gao, Y. Yang, H. Huang, P. Miao, Y. Liu, A. Chen, C. W. Nan, C. Gao, *Sci. Rep.* **2014**, *4*, 4591.

[5] H. Cao, F. Bai, N. Wang, J. Li, D. Viehland, G. Xu, G. Shirane, *Phys. Rev. B* **2005**, *72*, 064104.

[6] J.-M. Kiat, Y. Uesu, B. Dkhil, M. Matsuda, C. Malibert, G. Calvarin, *Phys. Rev. B* **2002**, *65*, 064106.

[7] D. Viehland, J. F. Li, *J. Appl. Phys.* **2002**, *92*, 7690.

[8] F. Bai, N. Wang, J. Li, D. Viehland, P. M. Gehring, G. Xu, G. Shirane, *J. Appl. Phys.* **2004**, *96*, 1620.

[9] R. R. Chien, V. H. Schmidt, C.-S. Tu, L. W. Hung, H. Luo, *Phys. Rev. B* **2004**, *69*, 172101.

[10] H. Liu, J. Chen, L. Fan, Y. Ren, Z. Pan, K. V. Lalitha, J. Rodel, X. Xing, *Phys. Rev. Lett.* **2017**, *119*, 017601.

[11] F. Fang, X. Luo, W. Yang, *Phys. Rev. B* **2009**, *79*, 174118.